Optical Engineering

OpticalEngineering.SPIEDigitalLibrary.org

Spatiotemporal laser speckle flowmetry based on elastic-walled U-shaped tubing apparatus: optical method for urinary flow measurement

Seungsoo Hong
Hyuntai Kim
Kyoungyoon Park
Youngchul Kwon
Hanbyul Chang
Songzhe Piao
Young Ju Lee
Seung-June Oh
Yoonchan Jeong

SPIE.

Seungsoo Hong, Hyuntai Kim, Kyoungyoon Park, Youngchul Kwon, Hanbyul Chang, Songzhe Piao, Young Ju Lee, Seung-June Oh, Yoonchan Jeong, "Spatiotemporal laser speckle flowmetry based on elastic-walled U-shaped tubing apparatus: optical method for urinary flow measurement," *Opt. Eng.* **57**(10), 104110 (2018), doi: 10.1117/1.OE.57.10.104110.

Optical Engineering 57(10), 104110 (October 2018)

Spatiotemporal laser speckle flowmetry based on elastic-walled U-shaped tubing apparatus: optical method for urinary flow measurement

Seungsoo Hong,[a] Hyuntai Kim,[b] Kyoungyoon Park,[a] Youngchul Kwon,[c] Hanbyul Chang,[a] Songzhe Piao,[d] Young Ju Lee,[e] Seung-June Oh,[e] and Yoonchan Jeong[a,f,*]

[a]Seoul National University, Laser Engineering and Applications Laboratory, Department of Electrical and Computer Engineering, Seoul, Republic of Korea
[b]University of Southampton, Optoelectronics Research Centre, Highfield, Southampton, United Kingdom
[c]Samsung Electronics, Test & Package Center, Asan, Republic of Korea
[d]Taizhou Hospital of Zhejiang Province, Department of Urology, Taizhou, China
[e]Seoul National University Hospital, Department of Urology, Seoul, Republic of Korea
[f]Seoul National University, ISRC & IAP, Seoul, Republic of Korea

Abstract. We propose an optical method for uroflowmetry, exploiting the laser speckle contrast imaging (LSCI) technique onto an intermediate tubing apparatus having an elastic wall that can sensitively respond to flow-induced shedding vortices. Based on the method, we devised and fabricated an elastic-walled U-shaped tubing apparatus (EWUSTA), using the three-dimensional printing technique. We utilized the spatiotemporal contrast scheme for the LSCI as a fast and reliable computational algorithm. We investigated three different materials of flex-vinyl, ninja-flex, and natural rubber latex for the elastic wall of the EWUSTA in steady flow conditions, and verified that their optimal operational ranges could extend up to 7, 15, and 25 ml/s, respectively. We characterized the natural-rubber-latex-based EWUSTA in dynamic flow conditions in comparison with a commercial reservoir-weight-transducer-based gravimetric flowmeter, and verified its feasibility. We stress that the proposed method can offer precise and accurate information on flow dynamics. In addition, we found that the upper limit of the optimal operational range of the proposed apparatus had strong correlation with the tensile strength of the elastic-wall material. We reckon that the proposed and demonstrated method has great potential not only for uroflowmetry but also for other flow-related medical and industrial applications. [DOI: 10.1117/1.OE.57.10.104110]

Keywords: laser speckle contrast imaging; laser speckle flowmetry; flow-induced vibration; vortex shedding; uroflowmetry.

Paper 181135 received Aug. 7, 2018; accepted for publication Oct. 4, 2018; published online Oct. 22, 2018.

1 Introduction

Storage and emptying of the urinary bladder is one of the most important basic physiologies of the human body. The micturition phenomenon is a result of an integral coordination of the urinary bladder, urethral sphincter, pelvic floor musculature, and nervous system.[1] Lower urinary tract dysfunctions are the most prevalent condition of the urological outpatient clinic.[2] The population having such voiding dysfunctions and urinary incontinence is increasing with ageing and degenerative neurological diseases. The most important diagnostic modality for evaluating them is urodynamic study, the very fundamental component of which is in fact uroflowmetry.[3]

Uroflowmetry is a noninvasive, fast, and inexpensive procedure, capable of providing useful information on the bladder voiding pattern, during which a patient is only able to empty his or her bladder either in standing or sitting posture. Due to such a simple procedure, it is performed for most patients, who visit the urological clinic for lower urinary tract dysfunctions as the first-line test.[4] To date, various types of uroflowmeters have been developed for uroflowmetry: the most common types of them are based on a weight meter with a reservoir (gravimetric measurement), a rotating disc, or an electronic dipstick.[5] With them, a patient under diagnosis is required to stand up in front of a micturition funnel or to sit down on a micturition chair, while emptying his or her bladder. However, these conventional uroflowmeters have some unresolved issues with patients having problems in urinating in a standing or sitting posture owing to various reasons, such as paraplegia, back pain, psychological discomfort, germ phobia, cortical inhibition, etc., thereby often failing to provide appropriate test results. In such cases, uroflowmetry may be performed more comfortably and correctly if a patient is allowed to empty his or her bladder in a lying posture through a urinary catheter with extension tubing that passes the urinary flow to a uroflowmeter placed at a distant from the patient. However, the flow rate can easily be distorted and delayed due to the long delivery section of the urinary tubing. Moreover, the degree of the distortion can also vary significantly, depending on the geometric conditions around the patient. Thus, an alternative method for uroflowmetry that does not necessarily rely on a long delivery procedure as well as being capable of avoiding using a bulky reservoir or a heavy electro-mechanical system is currently in high demand from the urological clinic.

Therefore, the purpose of this study is to develop an optical method for urinary flow measurement by exploiting laser speckle contrast imaging (LSCI) combined with a specially

*Address all correspondence to: Yoonchan Jeong, E-mail: yoonchan@snu.ac.kr

designed tubing apparatus. The latter was devised to convert the urinary flow into vortex-shedding-induced vibration, which subsequently results in a corresponding perturbation to the laser speckle pattern (LSP). This is because it is nearly impossible to apply LSCI directly onto the bare urinary flow due to the fact that it does not contain any significant amount of scattering centers capable of producing LSPs resolvable from the background image. We constructed a proof-of-principle instrument based on the proposed method, using a 650-nm laser diode, a charge-coupled device (CCD) camera, and a three-dimensional (3-D)-printed tubing apparatus. We successfully demonstrated its validity for the flow rate up to 25 ml/s, which is high enough for uroflowmetry. We discuss its performance characteristics in both steady and dynamic flow conditions in comparison with the benchmark results obtained by a conventional reservoir-weight-transducer-based gravimetric flowmeter (RWTB-GF).

2 Theory on Laser Speckle Contrast Imaging via Flow-Induced Vibration

When coherent light is reflected or diffused by an optically rough surface, one can observe a randomly distributed granular pattern of intensity distribution called a LSP. In fact, such an LSP results from highly complicated, constructive, and destructive interferences of coherent light.[6] When the surface moves, it causes subtle phase shift of the reflected or diffused light, thereby leading to both temporal and spatial fluctuation of the random intensity distribution. If this fluctuation is statistically quantified, it gives information on how fast the surface moves. Analyzing such an LSP, one can evaluate its contrast C_{LS}, i.e., the laser speckle contrast (LSC), spatially, temporally, or spatiotemporally,[7] which is normally defined as the following:

$$C_{\mathrm{LS}} = \frac{\sigma}{\langle I \rangle} = \frac{\sqrt{\langle I^2 \rangle - \langle I \rangle^2}}{\langle I \rangle}, \tag{1}$$

where σ and $\langle I \rangle$ denote the standard deviation and mean value of the pixel intensities, respectively. The LSC is in fact a function of the decorrelation time of the laser speckle τ_c, which is related to the decorrelation velocity v_c, such as Ref. 8:

$$v_c = \frac{\lambda}{2\pi\tau_c}(m/s), \tag{2}$$

where λ is the wavelength of the incident light. The decorrelation velocity is closely linked with the real velocity or the time change rate of the movement of the given medium, so that once the LSC is measured, the velocity or the time change rate of the movement of the medium can be determined in a relative manner.[9,10] Thus, LSCI can offer a powerful route for velocimetry as well as for flow visualization in various applications, most vividly in biomedicine.[7–10]

LSCI can directly be utilized in measuring the velocity of a fluidic flow as long as the flow contains a sufficient number of scattering centers per unit volume, so that they can produce resolvable LSPs.[11] Otherwise, one should measure the flow rate indirectly via detecting the vibration of a thin physical surface or wall that is in contact with the fluidic flow, because the movement of fluid tends to induce vortex shedding oscillation onto the contacting wall.[12] In general, the period of the vortex shedding oscillation τ_{vs} is inversely proportional to the flow velocity such as in Ref. 13:

$$\tau_{vs} = \frac{d}{St \cdot v}(s), \tag{3}$$

where St, v, and d denote the Strouhal number, the velocity of fluid, and the cross-sectional dimension of the passage of the flow (i.e., the diameter of tubing). If LSCI is applied onto the wall of the passage of the fluidic flow, this characteristic time constant τ_{vs}, must be strongly linked with the decorrelation time of the laser speckle τ_c.[14] Thus, as long as the wall is elastic and sensitive enough to respond to the vortex shedding oscillation induced by the fluidic flow, the LSCI measurement onto the vibrating wall can be an effective alternative method for measuring the velocity of the fluidic flow in contact with the wall.

In order to determine the corresponding LSC, we simply exploit the spatiotemporal method,[15] in which the LSC is directly calculated from a single set of the total number of $N_x \times N_y \times N_t$ pixels, where N_x and N_y denote the lengths of pixels in the spatial domain and N_t denotes the number of frames in the temporal domain. Unlike the conventional spatial, temporal, or spatiotemporal calculation methods used for *in-vivo* flow visualization,[7] we do not need to obtain any two-dimensional LSC map upon the LSCI measurement. This is because, in our case, the physical quantity to measure is the effective flow rate through the relatively thin urinary catheter tubing, so that it is unnecessary to figure out the velocity distribution over the cross-section of the tubing by the urinary flow. Consequently, the calculation procedure becomes very simple and straightforward, such that a single contrast value is obtained based on the single data set of $N_x \times N_y \times N_t$ pixels.

Once the LSC is experimentally measured, we need to correlate it with the real flow rate. The relationship between the LSC (C_{LS}) and the decorrelation time (τ_c) or the flow velocity (v) can be expressed by a variety of different prediction formulae, depending on the type of the statistical velocity distribution.[8] In general, a Lorentzian or Gaussian distribution is frequently assumed if light scattering is governed by diffusive or ballistic dynamics, respectively.[16] While one may consider some other types for the prediction of the velocity from the LSC,[17,18] we here consider Lorentzian and Gaussian velocity distributions in the first place. We will utilize both prediction formulae in comparison with the experimental data and decide which formula is more appropriate for our case in the following section. Both prediction formulae are given by Ref. 19:

$$C_{\mathrm{LS}}^2 = \beta\frac{e^{-2x} + 2x - 1}{2x^2} \text{ for a Lorentzian distribution} \tag{4}$$

or

$$C_{\mathrm{LS}}^2 = \beta\frac{e^{-2x^2} - 1 + \sqrt{2\pi}x \cdot erf(\sqrt{2}x)}{2x^2}$$

for a Gaussian distribution, (5)

where $x = T/\tau_c$, and T, β, and erf denote the exposure time, the loss or correction factor from the Siegert relation,[20] and the error function, respectively. Since we deal with the case of LSCI via the flow induced vibration, we additionally

introduce an empirical formula between the decorrelation time τ_c and the velocity of the fluidic flow v such as:

$$\tau_c = \frac{\alpha}{v}(s), \tag{6}$$

where α denotes a simple scaling constant to correlate τ_c with v.[21] While T is a given value, α and β have yet to be determined through calibration procedure in comparison with the reference data that should be obtained via separate measurement with a reference flowmeter of known characteristics, e.g., an RWTB-GF. The details of the calibration procedure will be discussed in Sec. 4.1.

3 Experimental Arrangement

As discussed in the preceding section, an elastic wall is now implemented into an intermediate tubing apparatus that can be connected to the conventional urinary catheter tubing. In fact, the flow characteristics obtained through this elastic wall may considerably vary with its geometrical form, dimension, elasticity, etc., on account of fluid–structure interactions.[22] Thus, we emphasize that an appropriate design of the tubing apparatus as well as a sensible choice of the elastic wall material are crucial in order to keep good linearity between the vortex shedding frequency (which is inverse of the period of the vortex shedding oscillation) and the flow rate [see Eq. (3)]. To fabricate appropriate and optimized tubing apparatus, we exploited 3-D printing technology, which is an additive manufacturing method used to create a 3-D object based on computer aided design (CAD). With the technology, a solid object can be constructed in almost any shape or geometry by successively adding materials layer by layer.[23] After having investigated a number of different designs of the tubing apparatus, we eventually reached a prototype design, which was based on the elastic-walled U-shaped tubing apparatus (EWUSTA), as shown in Fig. 1. We note that this prototype was actually one of the best designs that could lead to good sensitivity and linearity between the vortex shedding frequency and the flow rate. While we do not present them all in our current discussion, they included a V-shaped and I-shaped tubing apparatus with a variety of variations, for example. We empirically figured out that when we reduced the angle between the inlet water flow direction and the elastic wall, thereby leading to the V-shaped tubing apparatus or further to the I-shaped tubing apparatus, the sensitivity of the LSCI measurement was considerably reduced in comparison with the case with the U-shaped tubing apparatus.

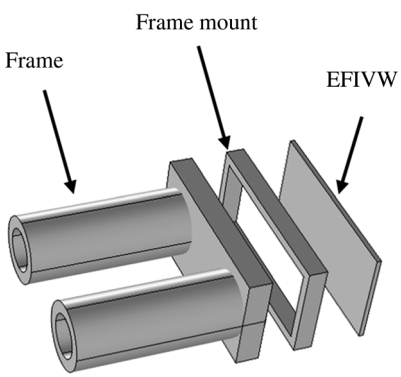

Fig. 1 Computer aided design image of the EWUSTA.

Table 1 Characteristic parameters of the three different materials for the EFIVW.

EFIVW material	FV[24]	NF[25]	NRL[26]
Thickness	0.13 mm	1 mm	0.15 mm
Tensile strength	20.5 MPa	26 MPa	30 MPa
Relative elasticity[a]	0.4	0.6 to 0.8	1
Break elongation	400%	500%	Over 600%

[a]Normalized relative to the elasticity of NRL.

The EWUSTA consisted of three parts: a frame with a pair of inlet and outlet tubing connectors, a frame mount, and an elastic wall, i.e., an elastic flow-induced-vibration wall (EFIVW). It was designed to be connected to urinary catheter tubing through the inlet and outlet ports. The frame with tubing connectors and the frame mount were 3-D printed with acrylonitrile butadiene styrene filaments. The dimensions of the frame mount were given by 40×20 mm^2, and the height and width of the frame mount were both 2 mm. We note that the height of the frame mount was carefully determined after iteratively testing a number of different heights. In addition, the EFIVW was prepared in three different materials, including flex-vinyl (FV), ninja-flex (NF), and natural rubber latex (NRL) as typical examples, the details of which are summarized in Table 1. We investigated these three different options for the EFIVW, comparing their performance characteristics in the following sections.

In Fig. 2, we illustrate the arrangement for our experiment. We declare that the purpose of our experiment was to demonstrate the feasibility of the proposed method, so that we conducted it in nonclinical environments and in room temperature conditions only, using laboratory water, instead of using real urine specimens. This was mainly because the physical properties of urine, including viscosity, do not considerably differ from those of water.[27,28] We note that, in general, the flow-induced vibration may be significantly dependent on the viscosity of the fluid; however, this aspect cannot be a concern, because the viscosity of urine is nearly the same as that of water, and it would not vary considerably with its specific condition in room temperature.[27,28] We controlled the flow rate of water by precisely adjusting the valve opening of the laboratory water supply and quantified it using a commercial RWTB-GF (Flowmaster, MMS), which had the specific flow rate resolution of 1 ml/s. More detailed experimental and computational procedures are summarized in the flowchart illustrated in Fig. 3. We used standard silicone rubber tubing with an inner diameter of 5 mm and a length of ~1.4 m to deliver the laboratory water into the inlet of the EWUSTA. We also used the same type of tubing of ~0.5 m to drain the water through the outlet port of the EWUSTA into the funnel-hopper assembly of the RWTB-GF, with which we determined the reference flow rates to calibrate the EWUSTA measurements. We note that while the cross-sectional diameter of the inlet tubing could modify the overall characteristics of the EWUSTA, it was not considered as a design parameter. This was because the cross-sectional diameter of the standard urinary catheter tubing is, in general, fixed to 5 mm. For LSCI, we set up a diode laser operating at 650 nm with

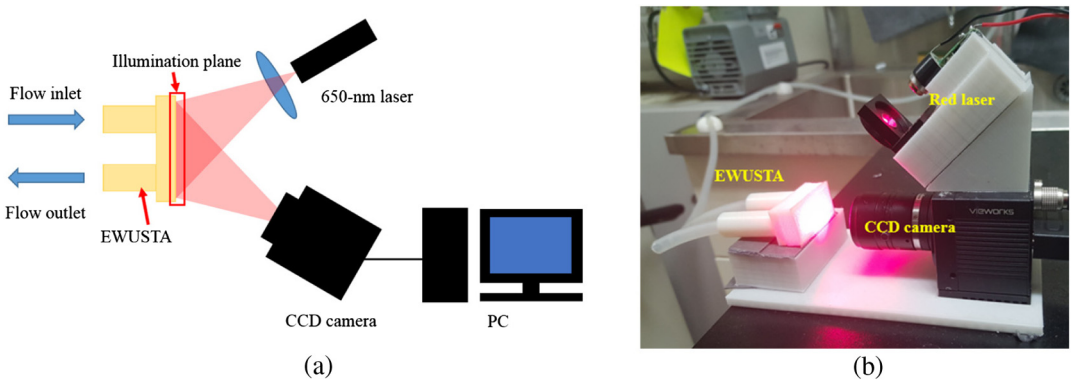

Fig. 2 Experimental arrangement for LSCI on the EWUSTA: (a) schematic of the experimental setup and (b) image of the real experimental setup.

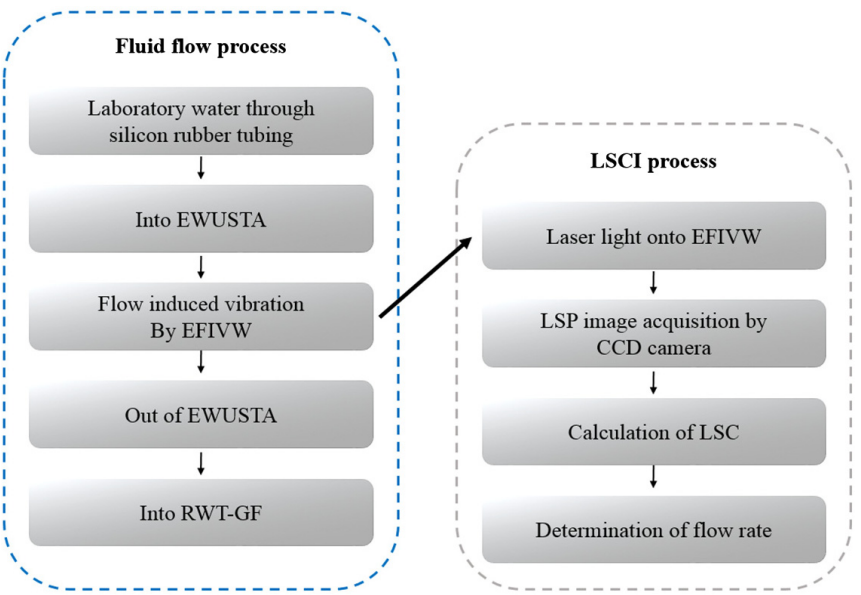

Fig. 3 Flowchart for the LSCI-based flow measurement.

50-mW output power (SDL650-50, SDLaser) to illuminate the surface of the EFIVW with coherent light, and a CCD camera (VH310C, VIEWorks) to obtain the LSP images from it. The linewidth of the diode laser was ~1 nm. The unit pixel size of the CCD camera was 7.4 μm, and the F-number of its imaging lens was 1.9. We note that we adjusted the magnification of the imaging setup in order that the typical speckle sizes became as large as at least two pixels of the CCD camera, satisfying the Nyquist criterion.[16,29] We also note that all the three materials tested for the EFIVW were nearly or completely opaque, so that no direct backscattered light from the water flow could contribute in the measured LSPs. The LSP image data were taken and processed by a personal computer (PC), using a commercial computational programming tool (MATLAB R2016b, MathWorks).

4 Experimental Results

4.1 *Spatiotemporal LSCI on EWUSTA in Steady Flow Conditions*

We first carried out spatiotemporal LSCI with the 3-D printed EWUSTA in steady flow conditions, investigating the three materials specified in Table 1 for the EFIVW. The general procedure for the spatiotemporal LSCI was as the following: we set the exposure time of the CCD at 10 ms, considering that the typical period of the vortex shedding oscillation was in the same order or significantly less than that.[30] While the full-size image taken by the CCD camera could be as large as 640×480 pixels, we only took 200×100 pixels positioned in the middle in order to eliminate undesirable fringing effects by the edge of the frame mount, to which the EFIVW was attached with adhesives. We took five images consecutively, so that the total number of $200 \times 100 \times 5$ pixels formed the single dataset for calculating the corresponding LSC under the spatiotemporal method.[7,21] In addition, the flow rate was also measured by the RWTB-GF at the same time for comparison and calibration purposes.

In Fig. 4, we illustrate typical snap shots of the LSPs recorded by the CCD camera from the EWUSTA with the three different EFIVW materials for different flow rates. While it may not be straightforward to perceive the precise contrast changes of the LSPs with respect to flow rate, one can notice that the LSPs became more blurred as the flow

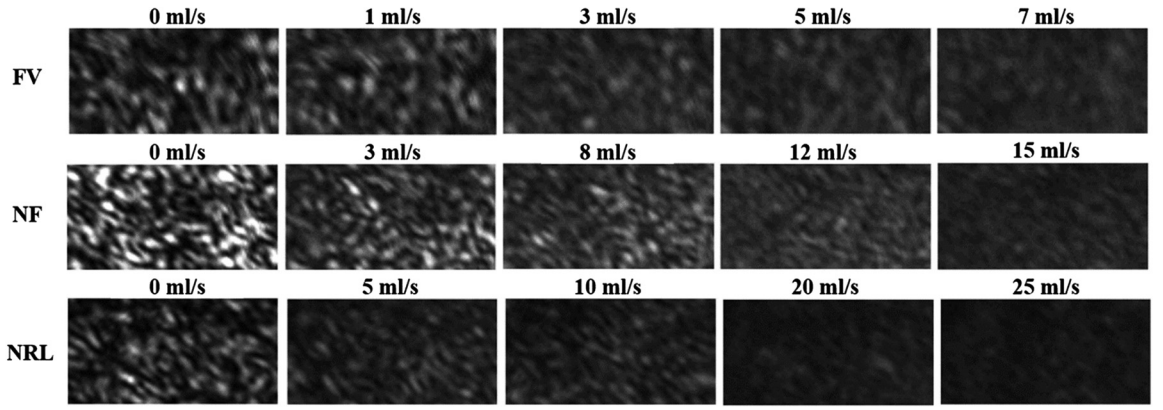

Fig. 4 Snap-shot images of the LSPs taken from the EFIVWs of FV, NF, and NRL for different flow rates, respectively.

rate increased, which implies the gradual reduction of the corresponding LSC.

In Fig. 5, we illustrate the experimentally measured LSC, i.e., C_{LS}, with respect to flow rate. We note that the flow rate was initially determined by the reference RWTB-GF. In the figure, we also plotted the fitting curves by the prediction formulae based on both Lorentzian and Gaussian distributions [see Eqs. (4) and (5)], for which we numerically obtained the two calibration factors of α and β for both cases, such that the root-mean-squared (rms) error of the prediction values against the experimental data points should be minimized with them. While both Lorentzian- and Gaussian-based prediction formulae could produce fitting curves matching well with the experimental data points, the latter performed better than the former for all three cases of the EFIVW materials. This means that the laser scattering process induced by the vibration of the EFIVW was governed mostly by ballistic (Gaussian) dynamics.[8,22] In addition, we noticed that the optimal operating range of the EFIVW significantly varied with the material kind: the maximal ranges were limited to 7, 15, and 25 ml/s for FV-, NF-, and NRL-EFIVWs, respectively. In other words, within the maximal ranges, the behaviors of EFIVWs could be predicted by the prediction formulae. This also means that within the ranges, the vortex shedding frequencies had sufficiently linear relationship with the applied flow rates [see Eqs. (3) and (6)]. However, once the flow rate exceeded the maximal ranges, its behavior could not be predicted or described by the given formulae. We suspect the limitation of the optimal operating range was due to the fact that if the EFIVW material was strained too much by hydraulic pressure, its deformation became inelastic.[31] We will discuss this matter in more detail in Sec. 5. All the measured and predicted values are summarized in Table 2, along with all the corresponding calibration parameters.

Nevertheless, the, NRL-EWUSTA exhibited superior performance over the other two in terms of the maximal range of the measurable flow rate, which we think must be sufficiently suitable for uroflowmetry applications. Hence, we hereafter chose the NRL-EWUSTA for further investigation in dynamic flow conditions.

4.2 *Spatiotemporal LSCI Based on NRL-EWUSTA in Dynamic Flow Conditions*

To verify the performance of the NRL-EWUSTA in dynamic flow conditions or in real-time measurement conditions, we arranged another set of experiment as the following: in general, a typical time scale for uroflowmetry is in the order of tens of seconds, so that we carried out the spatiotemporal LSCI onto NRL-EWUSTA in dynamic flow conditions for ~30 s as a typical example. In this case, we took consecutive

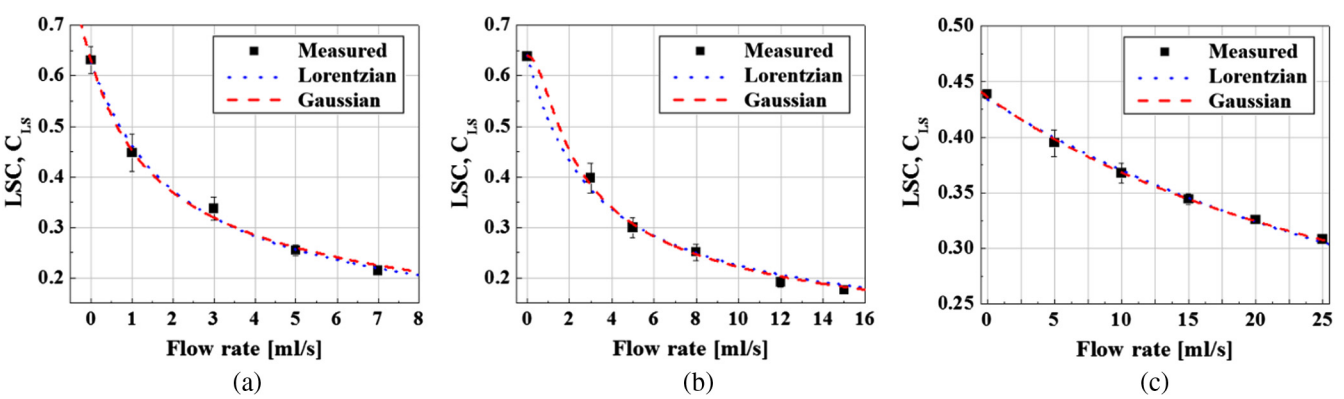

Fig. 5 LSCI measurement results in steady flow conditions, fitted with the prediction formulate based on Lorentzian (blue-dotted) and Gaussian (red-dashed) distributions: (a) FV-EWUSTA, (b) NF-EWUSTA, and (c) NRL-EWUSTA. The error bars denote the standard deviations of the total number of measurements of six times per point.

Table 2 LSC (C_{LS}) values with respect to flow rate for three different EFIVWs.

Flow rate (ml/s)		0	1	3	5	27	
FV	LSC (C_{LS}) $\alpha = 4.88 \times 10^{-1}$ $\beta = 6.59 \times 10^{-1}$	0.641	0.453	0.335	0.240	0.199	
Flow rate (ml/s)		0	3	5	8	12	15
NF	LSC (C_{LS}) $\alpha = 8.14 \times 10^{-1}$ $\beta = 4.49 \times 10^{-1}$	0.637	0.398	0.299	0.251	0.192	0.176
Flow rate (ml/s)		0	5	10	15	20	25
NRL	LSC (C_{LS}) $\alpha = 4.87$ $\beta = 7.66 \times 10^{-1}$	0.439	0.395	0.368	0.344	0.326	0.309

LSP images, using the CCD camera at 60 frames/s with its exposure time set at 10 ms, which means the temporal resolution of the dynamic LSC measurement was given by ~67 ms/measurement.

In addition, we also measured the flow rate of the water coming through the outlet port of the EWUSTA, using the RWTB-GF. Although this outlet flow might not be as identical as the inlet flow from the viewpoint of dynamic flow behavior, we think that it could still provide meaningful benchmarking data points. In general, water is nearly incompressible, so that as long as the water inside the tubing continues to flow and there is no leak in the passage, the flow rate should be preserved.[32] In order to minimize a possible flow distortion and delay by the extension tubing from the outlet port of the EWUSTA, we made it as short as ~0.5 m, placing the funnel-hopper assembly of the RWTB-GF as close as possible to the EWUSTA. All the other general procedures were as similar as those taken in the preceding section, except for synchronously recording all the data points from both the EWUSTA and the RWTB-GF. We prepared two sets of NRL-EWUSTA-I and NRL-EWUSTA-II in order to investigate them from the viewpoint of the reproducibility of performance. We note that while EWUSTAs could be 3-D printed in a nearly identical form, the NRL-EFIVWs were attached to them manually, so that the calibration factors for the normalized prediction formula had to be determined individually, such that $\alpha = 6.77$ and $\beta = 7.56 \times 10^{-1}$ for the former and $\alpha = 5.10$ and $\beta = 9.13 \times 10^{-1}$ for the latter, relying on the Gaussian-based formula. In Fig. 6, we illustrate the flow rates obtained by both NRL-EWUSTAs (blue traces) in dynamic flow conditions in comparison with those obtained by the commercial RWTB-GF (red traces).

From the illustrated results [see Figs. 6(a) and 6(d) at first], one can see that there were a couple of distinct features while the general trends of the dynamic response curves obtained by the NRL-EWUSTAs, including its overall shapes and levels, were matched well with those obtained by the RWTB-GF: first, the response curves by the NRL-EWUSTAs exhibited fast oscillating ripples, whereas those by the RWTB-GF did not. Second, there were some temporal shifts or delays between the two response curves, which varied considerably with time. As for the first distinct feature, the ripples in the response curves by the NRL-EWUSTAs might be due to the transient turbulences of the water flow inside the EWUSTAs, which in turn incurred the corresponding changes in the LSPs through the EFIVWs. In contrast, such behaviors were not apparent in the measurements by the RWTB-GF. One can explain this discrepancy in two folds: one is that abrupt or fast changes in the water flow might have been regulated physically by the ~0.5-m-length silicon-rubber tubing connected to the outlet port of the EWUSTA as well as the funnel-hopper assembly of the RWT-GF. The other is that they might have been regulated electronically by averaging the data points within a certain time interval in the case of the RWTB-GF. In fact, we experimentally observed that the RWTB-GF consistently could not resolve out any transient effects within a ~1.5-s interval even in direct measurement conditions. Thus, we suspect that the second explanation may well be plausible to some extent. In addition, if one regards that the fast oscillating ripples in the response curves by the NRL-EWUSTAs were artifacts caused by the transient turbulences of the water flow, one can readily remove them out via a simple electronic or numerical process, such as exploiting a low-pass filter or averaging the data points within a specific interval. The curves shown in Figs. 6(b), 6(c), 6(e), and 6(f) represent the results when we implemented both techniques, respectively. For the former, we applied a Gaussian low-pass filter with a cut-off frequency of 1.5 Hz in the full-width at half maximum to the original data directly obtained by the NRL-EWUSTAs. For the latter, we performed averaging for 30 consecutive data points (i.e., 0.5 s in terms of time interval) to determine the flow rate at a specific time. One can see that both techniques worked very well, efficiently eliminating the ripples, such that the resultant response curves look more matched with those by the RWTB-GF.

As for the temporal shift or delay feature, one can see that both response curves by the NRL-EWUSTAs precede those by the RWTB-GF by ~2 s at the initial stage. This was mainly due to the fact that the water flow arrived to the RWTB-GF through the ~0.5-m-length silicon-rubber tubing and a funnel-hopper assembly after going through the EWUSTA first. Thus, one may think that the time delay should simply be determined by the distance between the EWUSTA and the RWTB-GF, if one excludes any internal time delay by the RWTB-GF system itself. However, the measured discrepancy was not that simple. In particular, the time delay between the two responses was of ~2 s at

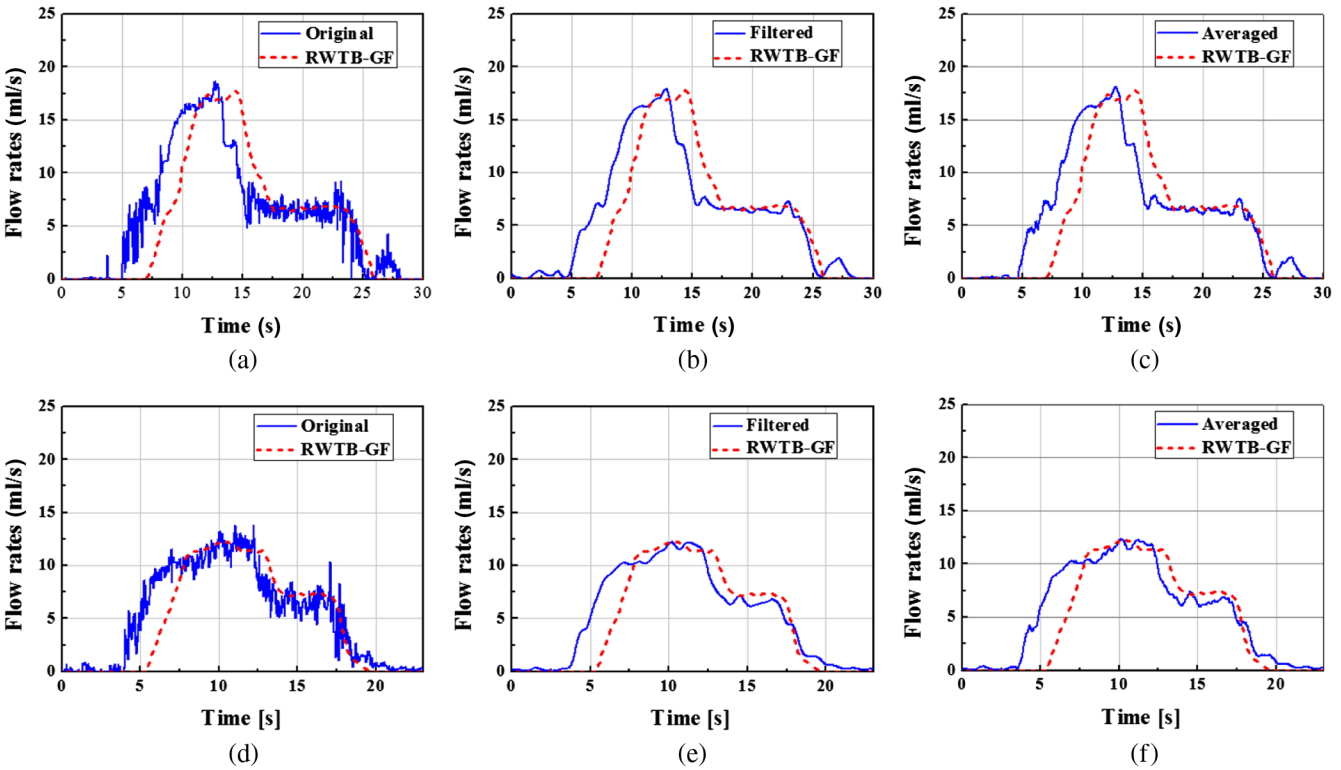

Fig. 6 LSCI measurement results in dynamic flow conditions: (a) NRL-EWUSTA-I with original data, (b) with 1.5-Hz-filtering, (c) with 30-point averaging; (d) NRL-EWUSTA-II with original data, (e) with 1.5-Hz-filtering, and (f) with 30-point averaging.

the opening stage, whereas it tended to be was reduced to ~0.5 s at the closing stage. This was due to the fact that as long as there was hydraulic pressure by the water supply in the drainage tubing, the measurement at the RWTB-GF was simply delayed by the time interval that the actual water flow took traveling the distance between the EWUSTA and the RWTB-GF. However, once there was no hydraulic pressure by the water supply to the EWUSTA, i.e., no water flow at the EWUSTA, the amount of water remaining within the drainage tubing attached to the EWUSTA could not continue to flow into the funnel-hopper assembly of the RWTB-GF. This was because water is essentially incompressible in normal conditions,[33] so that the water flow to the RWTB-GF was stopped nearly as soon as the valve of the water supply was closed. We note that this aspect may hit a critical issue for the RWTB-GF-based measurement unless the length of the urinary catheter tube is negligibly short, because the amount of urine being stuck within the urinary catheter tubing cannot be correctly weighed (or counted) by the RWTB-GF, thereby causing considerable underestimation of the total amount of urine to be measured. In fact, one can clearly observe the possible consequence from the curves illustrated in Fig. 7, in which we illustrate the aggregated amounts of water

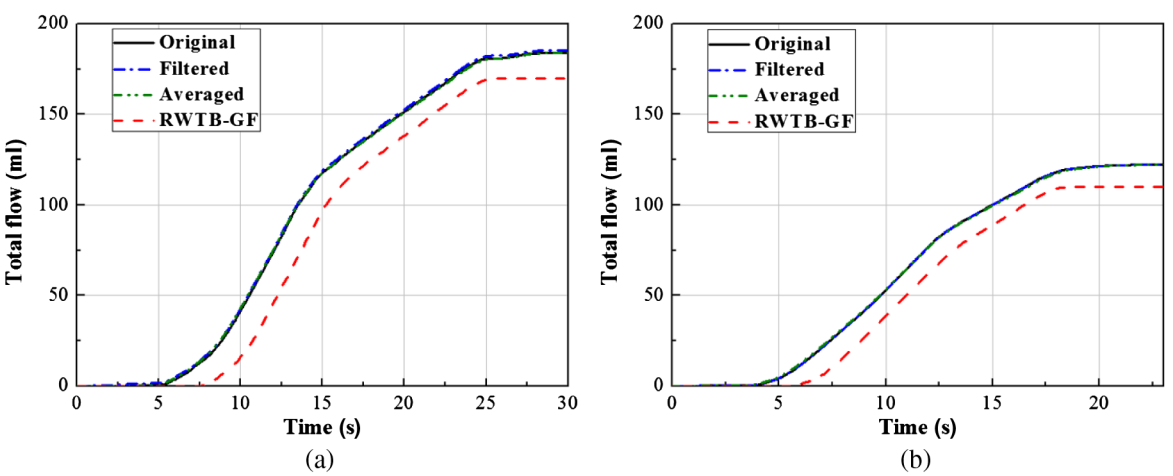

Fig. 7 Aggregated amounts of water measured by the EWUSTAs and the RWTB-GF: (a) obtained from Figs. 6(a)–6(c) and (b) obtained from Figs. 6(d)–6(f).

obtained from the EWUSTA and the RWTB-GF, respectively, integrating the flow rates shown in Fig. 6, with respect to time. One can see that there is a considerable gap of ~13 ml in the final values between the EWUSTA measurements and the RWTB-GF measurements for both cases. These measurement gaps indicate that there must be a certain amount of water remaining in the drainage tubing even after the flow rate had been reduced to zero, which we estimated to be ~11 ml, taking into account all the inner space of the EWUSTA and the drainage tubing between the EWUSTA and the RWTB-GF. We suspect that the small discrepancy between the measured and estimated gap values might be due to the transient response of the EFIVW of the EWUSTA to the abrupt hydraulic pressure change inside the tubing, as one can see that there are small side lobes or tails at $t = \sim 27$ s or $t = \sim 20$ s in Fig. 6(a) or Fig. 6(d), respectively, out of which we estimated that the discrepancies were given by ~2.5 ml and ~1.3 ml, respectively. Nevertheless, both EWUSTAs worked very well with near-identical performance, so that there remains no critical issue with reproducibility of performance.

5 Discussion

We devised an intermediate structure called EWUSTA to facilitate LSCI measurement of fluidic (or urinary) flow, where an EFIVW was supposed to convert the flow rate into the corresponding LSC. Our approach was performed under the assumption that the EFIVW responds linearly to the vortex shedding oscillation induced by the fluidic flow without considerable distortion. It has been verified with our experimental demonstrations that various elastic materials could satisfactorily be utilized as an EFIVW but with different optimal operational ranges: e.g., up to 7 ml/s with FV, 15 ml/s with NF, and 25 ml/s with NRL. Within the optimal operational ranges, the relationship between the flow rate and the vibration frequency remained linear, so that one could determine the flow rate from the measured LSC. For this, an extra procedure should be taken in order to determine the calibration factors of α and β [see Eqs. (4)–(6)]. We emphasize that the operational range up to 25 ml/s in the case of the NRL-EWUSTA should be high enough for uroflowmetry in most cases. We figured out that the maximal operational range was critically related with the elastic property of the EFIVW. In particular, as shown in Table 1, the tensile strength had strong correlation with the upper limit of the optimal operational range. The tensile strength is defined by the maximal strain, to which the linearity between stress and strain can hold.[34] In other words, up to the maximal strain point, the elastic or Young's modulus of the material remains constant. Thus, deformations of the material can completely be recovered upon removal of the strain as long as the applied strain is below the tensile strength. Otherwise, the deformations become irrecoverable, so that oscillatory deformations, i.e., vibrational motions tend to be anharmonic and nonlinear, as was observed in our experiments. In general, the tensile strength or elastic modulus is an inherent characteristic of a material irrespective of its geometric shape or condition.[26] Thus, the proper choice of the EFIVW material is crucial for elongation of the optimal operational range of the proposed method.

We stress that the issues with the RWTB-GF measurement observed and quantified in Figs. 6 and 7 in dynamic flow, conditions will become more serious if the length of the urinary catheter tubing is long or the strength of the urinary flow is weak, which is in fact a frequent situation with diagnosing various lower urinary tract dysfunctions.[2,35] In other words, when a conventional bulky reservoir-type flowmeter, such as the RWTB-GF we used as the reference flowmeter in the experiment, is placed at a distance from a patient with lengthy catheter tubing, the resultant uroflowmetry can give rise to significantly inaccurate outcomes, having large dependency of geometric conditions around a patient under diagnosis. In contrast, the proposed LSCI-based EWUSTA can be very effective for resolving out such issues, because it can be made relatively compact, being able to be placed very close to a patient under diagnosis.

We note that aging effects of the fabricated EWUSTA were not considerably noticed during the measurement. In fact, aging effects should not be a big issue, because we assume that the EWUSTA is a cheap disposable component, so that it is not necessarily supposed to be used multiple times if it is used under clinical conditions.

We finally note that the LSCI-based EWUSTA in the current investigation was built as a prototype, only utilizing commercial components and devices. As a result, the developed system had to be still a bit bulky in size and to be fixed in a stable location in order to perform the flow measurement properly. However, we think that this aspect can significantly be enhanced if we utilize more compact and custom-designed components and devices along with proper packaging or fiberization.[21,36] In fact, an optical computer mouse, which is actually based on the LSCI technology, is a good example indicating that a typical LSCI system has already dwindled down to the size of centimeters.[37] Therefore, there is enough potential that our device can be as small as an optical mouse. This will make the LSCI-based flowmeter portable and inexpensive, so that it can readily be utilized even at a patient's home. In such cases, patients who feel discomfort having a test at clinic can perform uroflowmetry for themselves with psychological comfort, which may lead to even better uroflow data acquisition.

6 Conclusion

We have developed an LSCI-based flowmeter with EWUSTA as an optical method for uroflowmetry. We verified its effectiveness and feasibility in both steady and dynamic flow conditions within flow rate up to 25 ml/s. Although it should need further improvement in terms of compact packaging and subsequent clinical studies, this method has great potential not only for uroflowmetry but also for other flow-related medical and industrial applications. Furthermore, one may also think of increasing the sensitivity of the system by exploiting an auxiliary speckled reference beam.[38]

Acknowledgments

This work was supported in part by the Interdisciplinary Research Initiatives Program from College of Engineering and College of Medicine, Seoul National University (Grant No. 2014-RSC01); National Research Foundation of Korea (NRF) grant funded by the Government of Korea (Grant No. 2017R1D1A1B03036201); Ministry of Trade, Industry and Energy (Project no. 10060150); and Brain Korea 21 Plus Program. The authors declare that there are no conflicts of interests.

References

1. W. C. Groat, "Integrative control of the lower urinary tract: preclinical perspective," *Br. J. Pharmacol.* **147**, S25–S40 (2006).
2. S. J. Oh, *Interpretation of Urodynamic Studies: A Case Study-Based Guide*, Springer Verlag, Singapore (2018).
3. K. Chun, S. J. Kim, and S. T. Cho, "Noninvasive medical tools for evaluating voiding pattern in real life," *Int. Neurourol. J.* **21**(Suppl 1), S10–S16 (2017).
4. W. Schafer et al., "Good urodynamic practices: uroflowmetry, filling cystometry, and pressure-flow studies," *Neurourol. Urofynamics* **21**, 261–274 (2002).
5. J. J. M. C. De La Rosette et al., "Improved reliability of uroflowmetry investigations: results of a portable home-based uroflowmetry study," *Br. J. Urol.* **78**, 385–390 (1996).
6. Y. Jeong and B. Lee, "Effect of random pattern through a multimode-fiber bundle on angular and spatial selectivity in volume holograms: experiments and theory," *Appl. Opt.* **41**, 4085–4091 (2002).
7. J. Qiu et al., "Spatiotemporal laser speckle contrast analysis for blood flow imaging with maximized speckle contrast," *J. Biomed. Opt.* **15**, 016003 (2010).
8. K. Basak, M. Manjunatha, and P. K. Dutta, "Review of laser speckle-based analysis in medical imaging," *Med. Biol. Eng. Comput.* **50**, 547–558 (2012).
9. A. B. Parthasarathy et al., "Robust flow measurement with multi-exposure speckle imaging," *Opt. Express* **16**, 1975–1989 (2008).
10. A. Humeau-Heurtier et al., "Multiscale compression entropy of micro-vascular blood flow signals: comparison of results from laser speckle contrast and laser Doppler flowmetry data in healthy subjects," *Entropy* **16**, 5777–5795 (2014).
11. S. Hong et al., "Laser speckle contrast imaging method for measurement of transparent fluid flows," in *Optical Sensors*, Zurich, Switzerland, pp. SeTh3E.2 (2018).https://doi.org/10.1364/SENSORS.2018.SeTh3E.2
12. S. Miwa, M. Mori, and T. Hibiki, "Two-phase flow induced vibration in piping systems," *Prog. Nucl. Energy* **78**, 270–284 (2015).
13. H. Cen, "Flow-induced vibration of a flexible circular cylinder," PhD Thesis, University of Windsor, Ontario, Canada (2015).
14. P. C. Li, C. J. Cheng, and C. K. Yeh, "On velocity estimation using speckle decorrelation," *IEEE Trans. Ultrason. Ferroelectr. Freq. Control* **48**, 761–768 (2001).
15. T. Durduran et al., "Spatiotemporal quantification of cerebral blood flow during functional activation in rat somatosensory cortex using laser-speckle flowmetry," *J. Cereb. Blood Flow Metab.* **24**, 518–525 (2004).
16. D. Briers et al., "Laser speckle contrast imaging: theoretical and practical limitations," *J. Biomed. Opt.* **18**, 066018 (2013).
17. A. F. Fercher and J. D. Briers, "A laser speckle technique for the visualization of retinal blood flow," *Proc. SPIE* **0369**, 22–28 (1982).
18. J. C. Ramirez-San-Juan et al., "Impact of velocity distribution assumption on simplified laser speckle imaging equation," *Opt. Express* **16**, 3197–3203 (2008).
19. R. Bandyopadhyay et al., "Speckle-visibility spectroscopy: a tool to study time-varying dynamics," *Rev. Sci. Instrum.* **76**, 93110 (2005).
20. P. A. Lemieux and D. J. Durian, "Investigating non-Gaussian scattering processes by using nth-order intensity correlation functions," *J. Opt. Soc. Am. A* **16**(7), 1651–1664 (1999).
21. L. Zhang et al., "Dual-wavelength laser speckle contrast imaging (dwLSCI) improves chronic measurement of superficial blood flow in hands," *Sensors* **17**, 2811 (2017).
22. R. Govardhan and C. H. K. Williamson, "Modes of vortex formation and frequency response of a freely vibrating cylinder," *J. Fluid. Mech.* **420**, 85–130 (2000).
23. M. Taufik and P. K. Jain, "Role of build orientation in layered manufacturing: a review," *Int. J. Manuf. Technol. Manage.* **27**, 47–73 (2013).
24. Microflex, "Vinyl exam gloves power-free," Product Literature, https://www.microflex.com (2017).
25. NinjaTek, "NinjaFlex 3D printing filament," *Technical Specifications*, https://ninjatek.com (2016).
26. K. Hanhi, M. Poikelispaa, and H. M. Tirila, *Elastomeric Materials*, Tampere University of Technology, Tampere (2007).
27. B. A. Inman et al., "The impact of temperature and urinary constituents on urine viscosity and its relevance to bladder hyperthermia treatment," *Int. J. Hyperthermia* **29**, 206–210 (2013).
28. R. Burton-Opitz and R. Dinegar, "The viscosity of urine," *Am. J. Physiol. Soc.* **47**, 220–230 (1918).
29. S. J. Kirkpatrick, D. D. Duncan, and E. M. Wells-Gray, "Detrimental effects of speckle-pixel size matching in laser speckle contrast imaging," *Opt. Lett.* **33**, 2886–2888 (2008).
30. S. Yuan et al., "Determination of optimal exposure time for imaging of blood flow changes with laser speckle contrast imaging," *Appl. Opt.* **44**, 1823–1830 (2005).
31. R. W. Ogden, *Non-Linear Elastic Deformations*, Dover Publications, New York (1997).
32. Y. Nakayama and R. F. Boucher, *Introduction to Fluid Mechanics*, Butterworth-Heinemann, Oxford (1998).
33. P. F. Fischer and A. T. Patera, "Parallel simulation of viscous incompressible flows," *Annu. Rev. Fluid Mech.* **26**, 483–527 (1994).
34. C. Lee et al., "Measurement of the elastic properties and intrinsic strength of monolayer graphene," *Science* **321**, 385–388 (2008).
35. S. Piao et al., "The in vivo effect of ytterbium-doped fiber laser on rat buccal mucosa as a simulation of its effect on the urinary tract: a pre-clinical histopathological evaluation," *Int. Neurourol. J.* **21**(Suppl 1), S17–S23 (2017).
36. H. Kim et al., "Corrugation-assisted metal-coated angled fiber-facet for wavelength-dependent off-axis directional beaming," *Opt. Express* **25**, 8366–8385 (2017).
37. P. Popov, S. Pulov, and B. A. Pulov, "A laser speckle pattern technique for designing an optical computer mouse," *Opt. Lasers Eng.* **42**, 21–26 (2004).
38. D. Li, D. P. Kelly, and J. T. Sheridan, "K speckle: space-time correlation function of doubly scattered light in an imaging system," *J. Opt. Soc. Am. A* **30**, 969–978 (2013).

Seungsoo Hong received his BS degree in electrical and electronic engineering from Yonsei University, Korea, in 2012. He is currently pursuing his PhD degree at the Department of Electrical and Computer Engineering, Seoul National University, Korea. He is primarily interested in laser imaging, including laser speckle contrast imaging and optical coherence tomography.

Hyuntai Kim received his PhD degree from the Department of Electrical and Computer Engineering, Seoul National University, Korea, in 2016. After having 1 year postdoctoral training at the same university, he joined the Optoelectronics Research Center at the University of Southampton as a research fellow in 2017. He is primarily interested in fiber optics and nanophotonics.

Kyoungyoon Park received his BS degree in electronic and electrical engineering from POSTECH, Korea, in 2012. His recent interests include nonlinear fiber optics and quantum optics. He is currently pursuing his PhD degree at the Department of Electrical and Computer Engineering, Seoul National University, Korea.

Youngchul Kwon received his PhD degree from the Department of Electrical and Computer Engineering, Seoul National University, Korea, in 2017. He is primarily interested in ultrafast optics and nonlinear fiber optics.

Hanbyul Chang received his BS degree in electrical engineering from Seoul National University, Korea, in 2015. He is primarily interested in fiber lasers and quantum photonics. He is now pursuing the PhD degree at the Department of Electrical and Computer Engineering, Seoul National University, Korea.

Songzhe Piao is a medical doctor and member of the Department of Urology, Taizhou Hospital of Zhejiang Province, China.

Young Ju Lee is a medical doctor and member of the Department of Urology, Seoul National University Hospital, Korea.

Seung-June Oh is currently a professor of urology, the College of Medicine at Seoul National University, Korea. He has authored or coauthored over 175 peer-reviewed papers, including 118 international journal articles and contributed to 12 book chapters, including a chapter in the 9th edition of Campbell's urology textbook as the first author. His primary interest is in benign prostatic hyperplasia (BPH), overactive bladder, and neuropathic lower urinary tract dysfunction.

Yoonchan Jeong obtained his PhD degree in 1999 from the School of Electrical Engineering, Seoul National University (SNU), Korea. He joined the Optoelectronics Research Center, University of Southampton in 2001 as a research fellow and became a reader in 2006. He returned to the Department of Electrical and Computer Engineering, SNU as a faculty member in 2010. His work in lasers and photonics has led to over 300 publications, including patents, book contributions, and journal/conference papers.